A Capacitance Type Chemical Sensor Based on $AlPO_4$-5 Molecular Sieves

Kenneth J. Balkus, Jr.,*,† Laura J. Ball,† Bruce E. Gnade,‡ and J. Mark Anthony‡

University of Texas at Dallas, Department of Chemistry, Richardson, Texas 75083-0688, and Materials Science Laboratory, Semiconductor Research and Development, Texas Instruments, Inc., Dallas, Texas 75265

Received January 23, 1996. Revised Manuscript Received September 19, 1996⊗

Thin films of $AlPO_4$-5 molecular sieves have been employed as the dielectric phase in a capacitance type chemical sensor. $AlPO_4$-5 was deposited onto titanium nitride (bottom electrode) coated silicon wafers by laser ablation. A subsequent hydrothermal treatment of the ablated $AlPO_4$-5 films was found to enhance the crystallinity. The capacitance sensor configuration was completed by the deposition of Pd/Au pads (upper electrode) through a mask. $AlPO_4$-5 based sensors exhibited significant changes in capacitance upon exposure to small molecules such as CO_2, CO, N_2, and H_2O.

Introduction

Molecular sieves are microporous, crystalline metal oxides.[1] The size and shape of these micropores determine which molecules can enter the cavities and/or channels which are sterically excluded. The selective adsorption properties of these materials have previously been exploited for chemical sensors based on mass,[2−6] optical,[7,8] and electronic changes.[9−19] Zeolite molecular sieves have shown promise in surface acoustic wave devices for the detection of large organic molecules such as pyridine and perfluorotributylamine in N_2. However, such devices are challenged by analytes of similar size and shape. Optical sensors that employ zeolites have been shown to detect NH_3, CO, H_2, C_2H_4, and N_2 but for NH_3 the zeolite had to be heated to 200 °C in order to be reversible.[7] In contrast, capacitance type chemical sensors measure a change in the dielectric properties such that one should be able to differentiate small molecules based on polarity. The adsorption of an analyte molecule should affect a signature change in the molecular sieve dielectric properties that can then be quantified by measuring the capacitance or impedance. An interdigitated capacitance device that incorporates NaY type zeolites was reported to measure capacitance changes in the picofarad range upon exposure to H_2O and butane.[9,10] We subsequently reported that a capacitance type chemical sensor that utilizes laser ablated molecular sieves as the dielectric phase exhibit capacitance changes as great as 8 orders of magnitude upon exposure to small molecules such as CO.[15] The fabrication of our sensor depends on the deposition of thin (200−300 nm), continuous films of molecular sieves onto a TiN substrate. The molecular sieve films were deposited onto the TiN substrate by pulsed laser deposition (PLD) or laser ablation.[15−19] A subsequent hydrothermal treatment was found to increase the crystallinity of the molecular sieve films. In this configuration, the TiN serves as the bottom electrode and a Au/Pd alloy patterned on top of the molecular sieve serves as the top electrode as shown schematically in Figure 1.

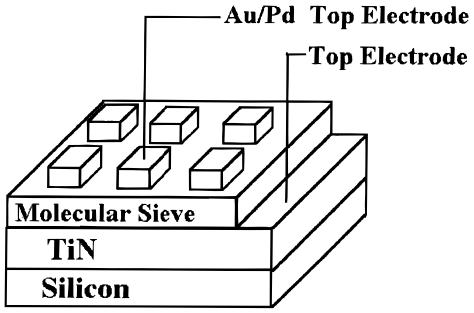

Figure 1. Schematic view of the $AlPO_4$-5 molecular sieve based sensor.

† The University of Texas at Dallas.
‡ Texas Instruments, Inc.
⊗ Abstract published in *Advance ACS Abstracts,* December 1, 1996.

(1) Szostak, R. *Molecular Sieves*; Van Nostrand Reinhold: New York, 1992.
(2) Brown, K.; Bien, T.; Fyre, G. C.; Bunker, C. J. *J. Am. Chem. Soc.* **1989**, *111*, 7640.
(3) Sun, J. T.; Dartt, C. B.; Davis, M. E. *Mater. Res Soc. Symp. Proc.* **1995**, *360*, 359.
(4) Yan, Y.; Bien, T. *Mater. Res. Soc. Symp. Proc.* **1991**, *233*, 175.
(5) Yan, Y.; Bien, T. *J. Phys. Chem.* **1992**, *96*, 9387.
(6) Yan, Y.; Bien, T. *Chem. Mater.* **1992**, *4*, 975.
(7) Ozin, G. A.; Kuperman, A.; Stein, A. *Angew. Chem., Int. Ed. Engl.* **1989**, *28*, 359.
(8) Coughlin, P. K.; Mercer, W. C.; Flanigen, E. M. U.S. Patent 4,927,768, 1990.
(9) Alberti, K.; Haaw, J.; Plog, C.; Fetting, F. *Catal. Today* **1991**, *8*, 509.
(10) Alberti, K.; Fetting, F. *Sens. Actuators* **1994**, *B21*, 39.
(11) Plog, C.; Maunz, W.; Kurzweil, K.; Obermeier, E.; Scheibe, C. *Sens. Actuators* **1995**, *B24−25*, 403.
(12) Kurzweil, K.; Maunz, W.; Plog, C. *Sens. Actuators* **1995**, *B24−25*, 653.
(13) Mercer, W. C.; Coughlin, P. K.; McLeod, Jr., D.; Flanigen, E. M. U.S. Patent 4,860,584, 1989.
(14) Mercer, W. C.; Coughlin, P. K.; McLeod, Jr., D.; Flanigen, E. M. U.S. Patent 4,876,890, 1989.
(15) Balkus Jr., K. J.; Ball, L. J.; Anthony, J. M.; Gnade, B. E., manuscript in preparation.
(16) Sottile, L. J.; Balkus, Jr., K. J.; Riley, S. J.; Gnade, B. E. *Mater. Res. Soc. Symp. Proc.* **1994**, *351*, 263.
(17) Balkus, Jr., K. J.; Riley, S. J.; Gnade, B. E. *Mater. Res. Soc. Symp. Proc.* **1994**, *351*, 437.
(18) Balkus, Jr., K. J.; Sottile, L. J.; Ngyuen, H.; Riley, S. J.; Gnade, B. E. *Mater. Res. Soc. Symp. Proc.* **1994**, *371*, 33.
(19) Balkus, Jr., K. J.; Ball, L. J.; Anthony, J. M.; Gnade, B. E., manuscript in preparation.

S0897-4756(96)00041-5 CCC: $14.00

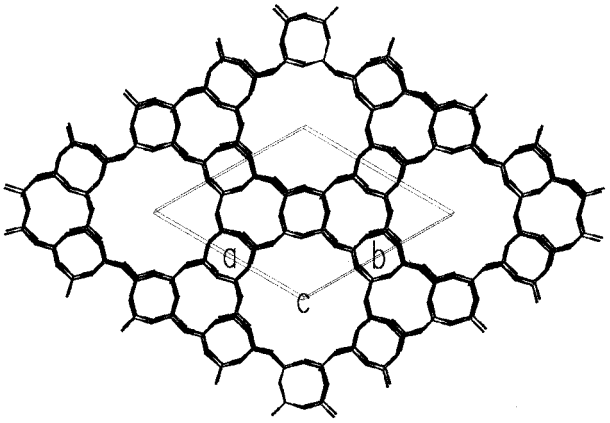

Figure 2. Framework structure of $AlPO_4$-5 viewed along the 100 direction.[20]

Voltage is applied between the electrodes, and the capacitance is measured. Exposure of the molecular sieve layer to different gases results in a change in capacitance.

In a preliminary account, we reported results for chemical sensors based on aluminum phosphate ($AlPO_4$) molecular sieves.[16−18] In particular, the large-pore, channel type $AlPO_4$-5 molecular sieve exhibited significant changes in capacitance upon exposure to N_2, H_2O, CO, CO_2, and toluene. In the present study, we report further results for the aluminum phosphate $AlPO_4$-5 based chemical sensor. The $AlPO_4$-5 structure is shown in Figure 2 and consists of four- and six-membered rings of alternating phosphate and aluminum ions bridged by oxygens.[20] These rings are arranged to produce one-dimensional channels 7.3 Å in diameter. $AlPO_4$-5 is thermally stable up to 700 °C, which implies a sensor based on this material could find application for the detection of combustion gases. For example, analysis of automobile exhaust would require stability to 600 °C prior to the catalytic converter and 300 °C after the catalyst. Important issues in developing a commercially viable sensor include sensitivity and reversibility. In this paper we evaluate reproducibility from both a response and fabrication standpoint as well as the sensitivity for CO and CO_2.

Experimental Section

Materials. $AlPO_4$-5 was synthesized according to the literature procedure[21] by first combining 4.50 mL of 85% H_3PO_4 with 22.42 mL of deionized water, followed by 5.83 g of $Al(OH)_3$ (83.34%). After stirring for 1 h, 6.30 mL of tripropylamine (TPA) was added to the mixture and stirred for an additional 1 h. The final gel composition had a molar ratio of $1.0TPA:1.0Al_2O_3:1P_2O_5:40H_2O$. The aluminum phosphate gel was transferred to a Teflon-lined autoclave (23 mL) and heated under static conditions at 150 °C for 20 h. The crystallization mixture was then cooled to room temperature, suction filtered, and washed with deionized water, and the $AlPO_4$-5 dried at room temperature.

The as-synthesized $AlPO_4$-5 was characterized by X-ray diffraction (XRD) and scanning electron microscopy (SEM). The XRD patterns were obtained using a Scintag XDS 2000 diffractometer with a scan rate of 1° min^{-1} and a chopper increment of 0.01. The scanning electron micrographs (SEM) were obtained by using a JEOL JSM 840A SEM. The Rutherford backscattering spectroscopy (RBS) was obtained by a National Electrostatics 3SDH tandem accelerator. The thickness measurements and Al/P atomic ratios were determined by a Rigaku 3550 wavelength-dispersive X-ray fluorescence system. The gases used in the capacitance measurements were as follows: 99.999% purity dry N_2, 99.998% purity CO_2, 50 ppm CO_2 in balance with 99.99% purity N_2, 99.998% purity CO, and 100 ppm CO in balance with 99.998% purity N_2.

Thin-Film Preparation. $AlPO_4$-5 targets for laser ablation were prepared by pressing ∼1 g of molecular sieve resulting in a pellet 1 in. in diameter and 0.25 in. thick. The experimental procedure for pulsed laser deposition of the molecular sieves has previously been discussed.[15−19] A Lumonics Hyper EX-400 excimer laser (KrF, 248 nm) was used for the ablation of $AlPO_4$-5. The laser fluence at the target was 9 J/cm^2 and a power density of 10^7 W/cm^2. Laser pulse energies measured by a Scientech calorimeter connected to a voltmeter varied from 50 to 90 mJ. A 10 ns pulse with repetition rates of 5−10 Hz were employed in this study. The ablated molecular sieves were deposited on a section of a silicon disk (∼1 cm^2) coated with a layer of titanium nitride (500 Å). The laser beam was reflected off a rastering mirror which was controlled by a computer that allowed the beam to move across the target instead of ablating material from a single spot. The beam was reduced by a 10 in. focal length convex lens to a 1 mm size spot on the target. The beam enters the ablation chamber through a fused silica window and then contacts the target mounted at an angle of 35° relative to the beam. The substrate was mounted on a heated stage at a distance of 1.5 cm from the target. Substrate temperatures over the range of 150−350 °C were studied. All depositions were made under a partial oxygen pressure of 0.55 Torr.

Sensor Measurements. Capacitors were prepared from titanium nitride on silicon wafers coated with ablated $AlPO_4$-5 molecular sieve films. The TiN served as the bottom electrode, while the top electrode was generated by vapor deposition of a Au/Pd alloy using a Denton Desk Lab II through a shadow mask with a thickness of 200 nm. The dielectric phase of all the capacitors were calcined at 400 °C to remove the organic template before depositing the top electrode.

Capacitance and current measurements were performed on a custom probe station as previously described.[16,18] The probe station was equipped with a microscope for viewing the probe tip placement and a gas manifold for controlling the atmosphere. Capacitance and current data were collected using a Keithley 237 voltage source and a Hewlett-Packard 4284A Precision LCR Meter. The probe chamber was equipped with one active and one ground probe controlled by micrometers.

All capacitance measurements were taken from the standpoint of having a capacitor in series with a resistor (Cs−RSV). The typical voltage range was −0.3 to +0.3 V. The ac frequency of the current applied to the capacitor was set at a specific oscillation frequency (0.1 kHz). The voltage range was divided into 10 data points during the measurement. Capacitance or current data from the five readings were averaged for each voltage point taken. All measurements were made at room temperature.

The leakage current was determined by taking current measurements. The current was set at a static 0.1 A, and the voltage range was set equal to that of the capacitance measurement being made (−0.3 to +0.3 V). The voltage range was again divided so as to produce 10 data points. The breakdown voltage was determined by scanning the voltage from 0 to 10 V and observing a significant increase ($>10^{-10}$ A/mm^2) in the current.

Results and Discussion

Thin-Film Preparation. We have previously reported the laser ablation of $AlPO_4$-5 molecular sieves onto a conductive surface.[16−18] It was found that a thin, continuous, and uniform $AlPO_4$-5 film can be obtained

(20) Bennet, J. M.; Cohen, J. P.; Flanigen, E. M.; Pluth, J. J.; Smith, J. V. *ACS Symp. Ser.* **1983**, *218*, 109.
(21) Wilson, S. T.; Lok, B. M.; Flanigen, E. M. U.S. Patent 4,310,440, 1982.

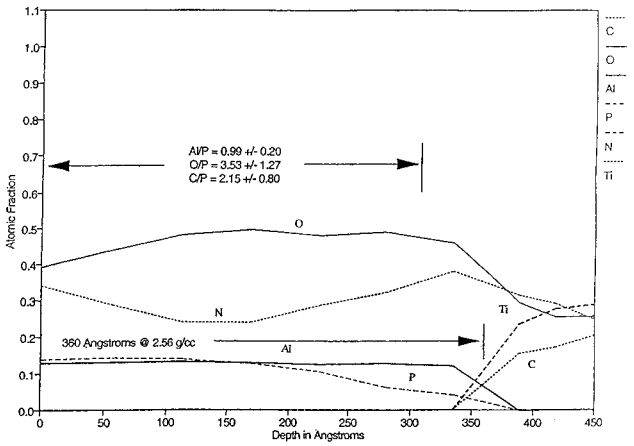

Figure 3. RBS depth profile of ablated $AlPO_4$-5 onto TiN.

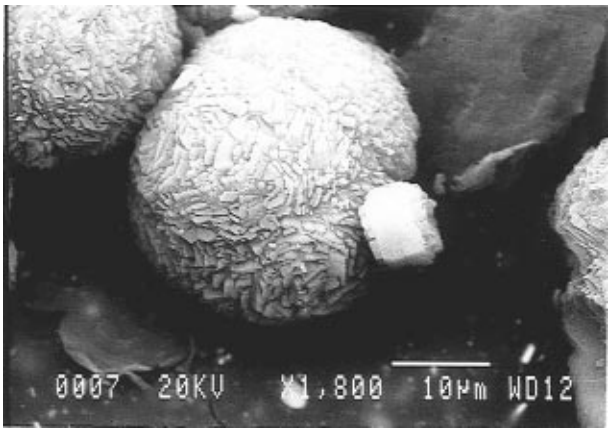

Figure 4. SEM of $AlPO_4$-5 target material.

by this deposition method[17,18] and that an increase in ablation time results in an increase in thickness of the metal oxide film. Furthermore, we have found that a hydrothermal treatment of 2 h at 150 °C in an $AlPO_4$-5 precursor gel enhances the crystallinity by rearranging the surface of the ablated films.[16−18] In the present study we have examined the pulsed laser deposition of $AlPO_4$-5 molecular sieves in more detail. In particular, we address the reproducibility of thin-film formation.

A Rutherford backscattering depth profile of an ablated 36 nm thick $AlPO_4$-5 film onto TiN is displayed in Figure 3. The parameters for the preparation of this sample were the following: 81 mJ, 10 Hz, substrate temperature 300 °C, O_2 pressure 0.5 Torr, and a deposition time of 10 min. A substrate temperature of 300 °C was used because below 160 °C using the above ablation conditions, the $AlPO_4$-5 did not adhere to the wafer surface. In the RBS spectrum the measure of oxygen is low by 15−20% because the helium scattering cross section is non-Rutherford at 2.4 Mev. The RBS indicates an the Al/P ratio of 0.99, which is consistent with the Al/P ratio of 1.0 for the $AlPO_4$-5 target material. This is in contrast to our previous studies, where we used much higher laser powers and the resulting ablated surfaces were aluminum rich. This may reflect the particulate number density which increases rapidly with increasing laser power,[22] resulting in the formation of amorphous aluminum oxides. The RBS also indicates the presence of carbon on the $AlPO_4$-5 film, which originates from the template (TPA) used in making the $AlPO_4$-5 target material. The presence of intact TPA has been confirmed by FT-IR spectroscopy.[23] We have previously shown that the hydrothermal treatment of ablated $AlPO_4$-5 improved the crystallinity without increasing the thickness. The presence of template in the target and subsequently in the ablated films is important, because if the template is removed from the $AlPO_4$-5 target prior to ablation, then the resulting films cannot be reorganized to $AlPO_4$-5. Instead dense phases such as tridymite are formed.[23]

The laser-deposited films generally appear amorphous as determined by X-ray powder diffraction. This is especially true when the target is composed of small crystals (<1 μm). A relationship between target crystal size and the crystallinity of the ablated films has not been firmly established in this case; however, there should be a higher probability of exfoliation with large crystals. Figure 4 shows a scanning electron micrograph of the $AlPO_4$-5 target material used in this study which indicates that the crystals are small (<1 μm) and form spherical aggregates.

The morphology of the ablated films does not appear to be influenced by the target crystallite size or shape. Figure 5 shows a 250 nm thick $AlPO_4$ film deposited directly onto silicon for better contrast. The cross-section view (Figure 5a) shows a fairly uniform and continuous film having a fibrillar structure which is more obvious from the surface view (Figure 5b). The estimated surface roughness of this film is ±∼15 nm.

The nature of the target surface also affects the morphology of the resulting $AlPO_4$ films as shown in Figure 6, where the film is irregular with large spherical deposits. In this case, the target had been used for several hours during which time the target surface eroded by repetitive laser ablation, forming long needle-shaped microstructures a few microns in size on the target. Mechanically, the target surface becomes very fragile and can be broken away by the thermal shock induced during the intense laser irradiation. This process of exfoliation results in loose debris which is carried toward the substrate by the rapidly expanding plume and condenses onto the thin film. Therefore, to consistently prepare uniform depositions, the films were deposited from a fresh target or the target was polished between ablations.

We propose that the ablated $AlPO_4$ films are composed of molecular sieve fragments that retain the organic template (TPA). These fragments can subsequently be reorganized under hydrothermal conditions without an increase in thickness. We have previously reported that hydrothermal treatment of ablated $AlPO_4$ phases can result in as much as a 20% increase in crystallinity.[15−19] The effects of a hydrothermal treatment depend on the nature of the molecular sieve as well as the morphology of the surface. Additionally, the presence of organic additives (template) influences how the surface fragments reorganize, such that for calcined $AlPO_4$ phases, the hydrothermal treatment results in dense phases or different molecular sieves compared with the target. Therefore, the template-containing molecular sieve film that is largely amorphous to XRD seeds the surface and reorganizes under hydrothermal conditions that might not otherwise produce that phase.

(22) Chen, L. C. In *Pulsed Laser Deposition of Thin Films*; Chrissy, D. B., Hubler, G. K., Eds.; John Wiley and Sons: New York, 1994; p 476.

(23) Riley, S. J. M.S. Thesis, University of Texas at Dallas, 1994.

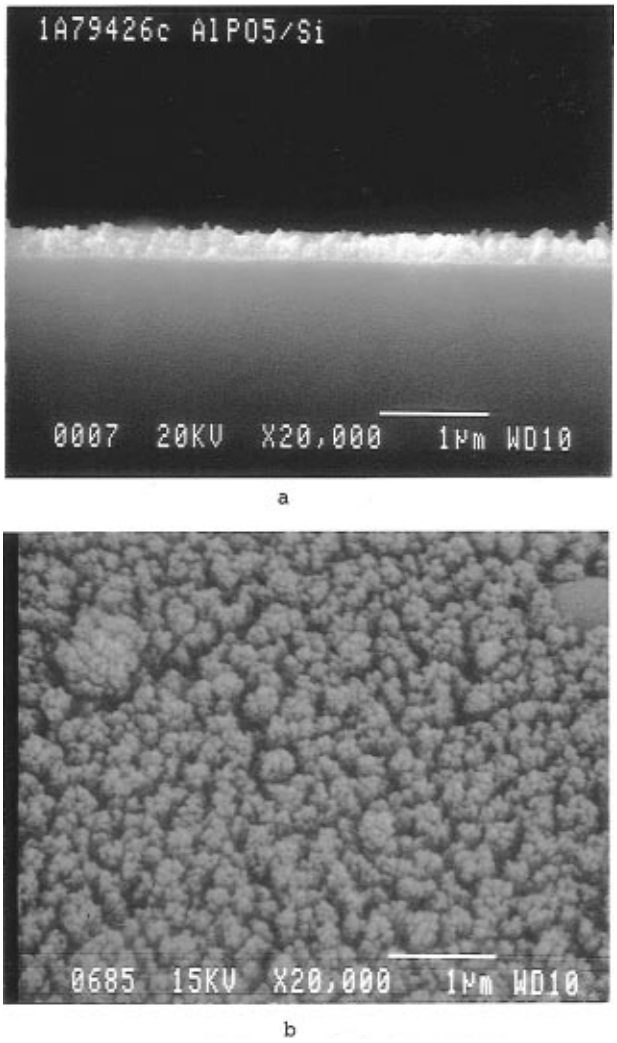

Figure 5. SEM of ablated $AlPO_4$-5 film on silicon deposited using 100 mJ, 10 Hz, and a deposition time of 20 min: (a) cross section and (b) surface view.

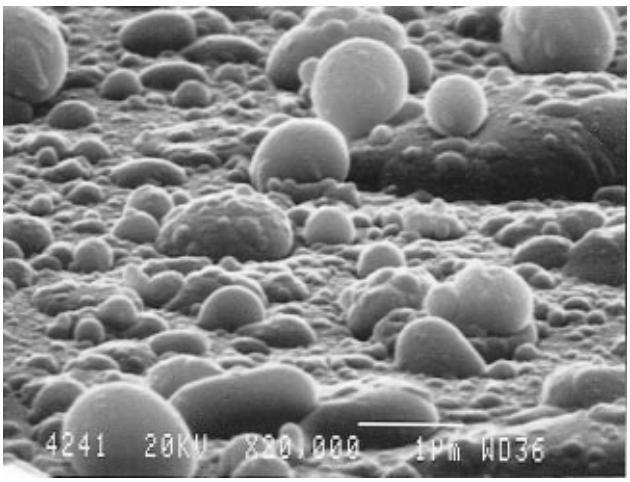

Figure 6. SEM of ablated $AlPO_4$-5 produced from a target used for several hours.

A report of a "memory" associated with the reactivity of amorphous films obtained from sputtered zeolites is consistent with our observation. [24]

The ablated $AlPO_4$-5 samples used to prepare the chemical sensors were hydrothermally treated for 2 h, which is long enough to increase the crystallinity without increasing the thickness. Figure 7 shows the XRD pattern of an ablated film that was hydrothermally treated in an $AlPO_4$-5 gel at 150 °C for 2 h. The X-ray diffraction pattern clearly indicates the presence of $AlPO_4$-5, which corresponds to an estimated 19% crystallinity relative to the target material which is probably on the low side because the film is only 312 nm thick. The XRD pattern also indicates there are no other detectable crystalline phases. X-ray diffraction analysis of the bulk powder produced from the gel used in the hydrothermal treatment indicated only amorphous $AlPO_4$ was present. This provides further evidence that the ablated surfaces are composed largely of molecular sieve fragments that reorganize and seed the gel mixtures during hydrothermal treatment. Figure 8 shows a cross-section view SEM of an ablated $AlPO_4$-5 surface after hydrothermal treatment. A comparison with Figure 5 indicates a loss in the fibrillar structure with formation of a more dense film after hydrothermal treatment. This reorganization to a more crystalline and continuous surface is an important feature of the thin films needed for the capacitance device. However, one can also envision applications in catalysis and separations for such molecular sieve films.

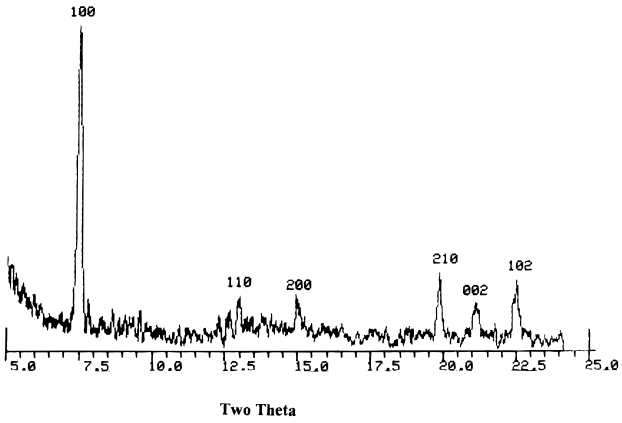

Figure 7. XRD pattern of hydrothermally treated $AlPO_4$-5 (312 nm thick).

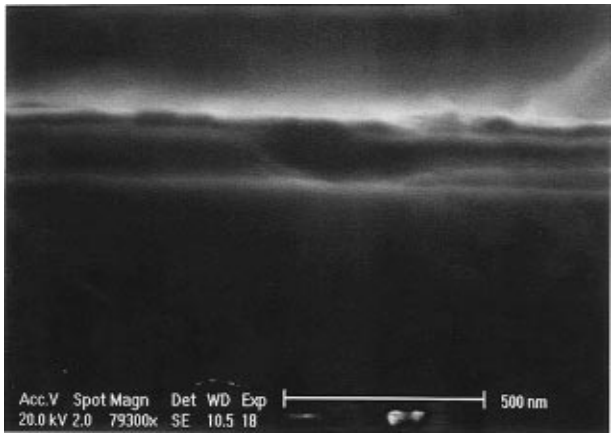

Figure 8. SEM of hydrothermally treated $AlPO_4$-5 (312 nm thick).

Sensor Measurements. We have previously reported the differences in selectivity in terms of capacitance changes between $AlPO_4$−H1, $AlPO_4$−H3, $AlPO_4$-5, CoAPO-5, MnAPO-5, VAPO-5, and MAPO-36 molecular sieve films which reflect the structural and compositional variance.[15−19] For example, water (ki-

(24) Boszormenyi, I.; Nakayama, T.; McIntyre, B.; Somarjai, G. A. *Catal. Lett.* **1991**, *10*, 343.

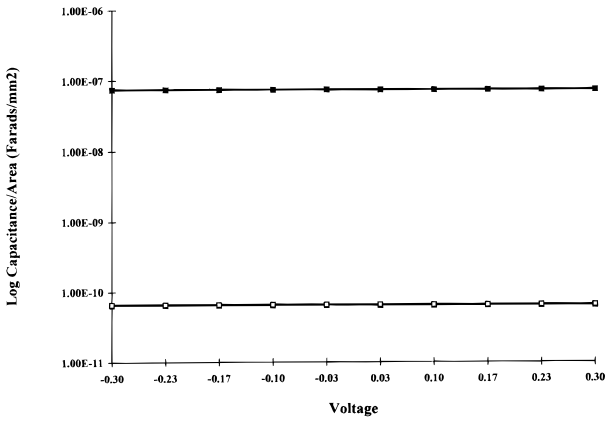

Figure 9. Plot of log capacitance/area (farads/mm^2) versus applied voltage (V) for $AlPO_4$-5 after room-temperature exposure to pure N_2 (△), exposed to pure CO_2 (■), and purged with pure N_2 (□) (320 nm thick and 10^{-12} A/mm^2).

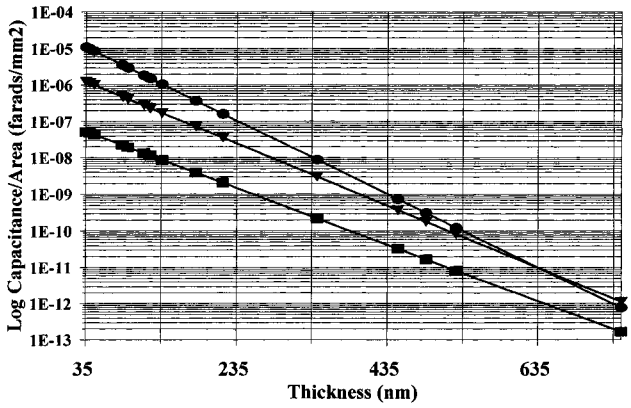

Figure 10. Plot of log capacitance/area (farads/mm^2) versus thickness of the $AlPO_4$-5 film after room-temperature exposure to pure N_2 (■), pure CO_2 (▼), and pure CO (●).

netic diameter of 2.65 Å) is readily adsorbed by the small-pore $AlPO_4$−H3 phase (3.5 × 3.7 Å). However, small molecules such as CO (kinetic diameter of 3.8 Å) or CO_2 (kinetic diameter of 3.3 Å) do not cause a change in capacitance when exposed to $AlPO_4$−H3, demonstrating a size exclusion effect. $AlPO_4$-5 has a larger pore size of 7.3 Å and as a consequence readily adsorbs small molecules such as CO, CO_2, N_2, O_2, and water so that selectivity will depend more on dipolar interactions with the oxide surface. Therefore the gas selectivity of a particular molecular sieve will depend on the size and shape of the analyte as well as the energy of interaction. This energy may reflect contributions from dispersion, repulsion, and polarization as well as dipole and quadrupole interactions.[25] In the present study, we focus on how the thickness of the $AlPO_4$-5 effects the capacitance changes and the leakage current. Furthermore, we have addressed the reversibility of the $AlPO_4$-5 based sensor *during* the detection of H_2O, CO_2, and CO. The sensitivity of the $AlPO_4$-5-based chemical sensor to CO and CO_2 has also been studied.

Figure 9 shows a typical plot of capacitance per area (farads/mm^2) versus applied voltage for $AlPO_4$-5 (320 nm thick and a leakage current of 10^{-12} A/mm^2). The potential range for this experiment was +0.3 to −0.3 V. Breakdown was typically observed above 1 V which was determined by a rapid increase in leakage current. For this film the capacitance upon exposure to pure N_2 at atmospheric pressure was measured to be 6.5×10^{-11} farads/mm^2, which is well above the background level of 10^{-14} farads/mm^2. When this sensor is exposed to pure CO_2, the capacitance increases to 10^{-8} farads/mm^2. The response time is as fast as we can make the measurements, which is a few minutes. We observe no further increase in capacitance after the initial measurement, suggesting the response time is faster than we can measure so far. Purging the system with pure N_2 at room temperature for several minutes restores the capacitance to approximately the original value (overlayed in Figure 9). These results show that laser-ablated $AlPO_4$-5 functions as a reasonable dielectric phase in a capacitor and that the adsorption of different gases of similar size (CO_2 kinetic diameter of 3.3 Å and N_2 kinetic diameter of 3.6 Å) causes changes in capacitance that are significantly different.

Figure 10 shows plots of capacitance per area (farads/mm^2) versus thickness of the deposited $AlPO_4$-5 film at a potential of +0.3 V. Since $C = A\epsilon/d$ (C = capacitance, A = area of the plate, ϵ = electric permittivity, and d = distance between the plates) we expected the capacitance to decrease as the thickness of the $AlPO_4$-5 dielectric phase increased. The gases used in this plot were pure N_2, CO_2, and CO at atmospheric pressure and room temperature. The capacitance changes between gases also decreased as the thickness increased which was similar for CoAPO-5.[15] The CO/CO_2 ratio for a 35 nm thick $AlPO_4$-5 based sensor is 10 while at 720 nm it is 1. This suggests that not only are thin films required to achieve a measurable capacitance changes but also thin films improve selectivity. The greater change in capacitance with CO is consistent with stronger interactions with the oxide surface. However, CO_2 has a smaller kinetic diameter than CO such that one might expect higher CO_2 adsorption. Therefore, the decreasing CO/CO_2 capacitance ratio with increasing thickness may reflect some contribution from the bulk dielectric properties of the gases. However, this effect should not be significant since the dielectric constants of CO and CO_2 are not dramatically different which means that there are other factors involved.

It is clear from Figure 10 that the thinnest films provide the greatest capacitance changes; however, as Figure 11 shows, the leakage current also increases. As the thickness increases, the leakage current decreases; thus, with sensors that have a thick dielectric phase the measurements appear more consistent. Therefore, we determined that a thickness of 200 to 300 ± 30 nm is preferred for our capacitance type sensor. The change in leakage current with thickness could also account for the slopes in Figure 10 which do not indicate a 1/d dependence.

Since we are interested in the detection of combustion gases, we have to be concerned with potential interference from water. Therefore, capacitance measurements were taken after the adsorption of H_2O followed by purging with N_2. A capacitor with a dielectric phase thickness of 320 nm was exposed to five N_2/H_2O cycles. Figure 12 shows a plot of the capacitance/area (farads/mm^2) for nitrogen (N_2-1) adsorption, then exposure to water vapor for 10 min (H_2O-1), followed by the capacitance change after a nitrogen purge for 10 min (N_2-2),

(25) Breck, D. *Zeolite Molecular Sieves*; R. Krieger Publishing: Malabar, FL, 1984.

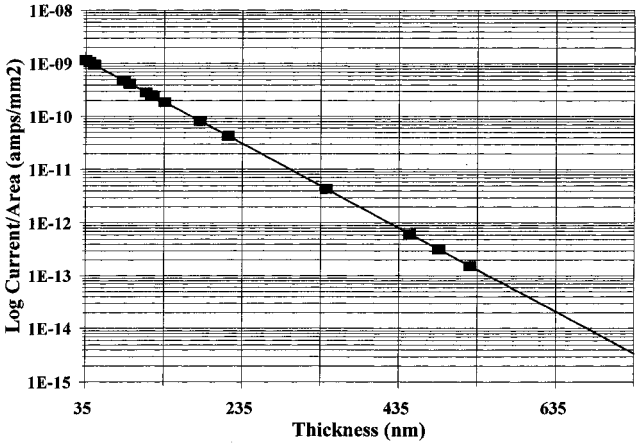

Figure 11. Plot of log current/area (A/mm^2) versus applied voltage (V) for $AlPO_4$-5 after room-temperature exposure to pure N_2 (■).

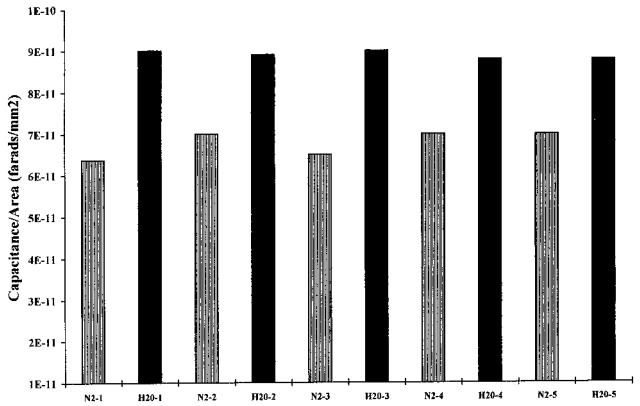

Figure 12. Plot of capacitance/area (farads/mm^2) for five room-temperature N_2/H_2O adsorption cycles by $AlPO_4$-5 (320 nm thick and 10^{-12} A/mm^2).

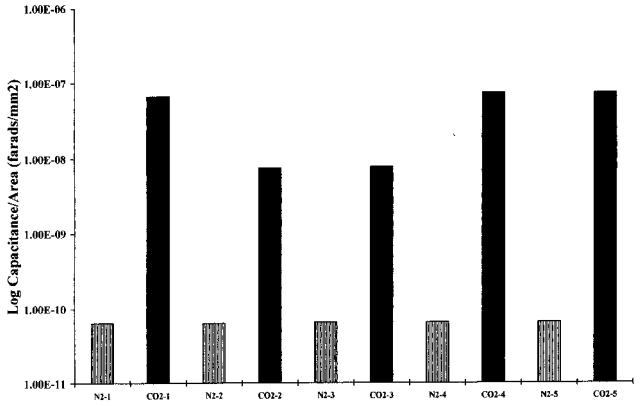

Figure 13. Plot of capacitance/area (farads/mm^2) for five room-temperature N_2/CO_2 adsorption cycles by $AlPO_4$-5 (320 nm thick and 10^{-12} A/mm^2).

etc., at a potential of +0.3 V. The average capacitance with a nitrogen purge was $(6.8 \pm 0.3) \times 10^{-11}$ farads/mm^2. The average capacitance after water is adsorbed in the dielectric phase was $(8.9 \pm 0.01) \times 10^{-11}$ farads/mm^2. Water is more polar than CO or CO_2, and therefore a higher capacitance was expected in a humid environment. However, atmospheric moisture will not interfere with the detection of CO_x gases since the change of capacitance for H_2O adsorption is considerably less than that for the adsorption of CO or CO_2 (vide infra). The response time for these measurements is probably less than 10 min, but we wanted to make sure that the molecular sieves were completely saturated in order to achieve the largest capacitance change possible.

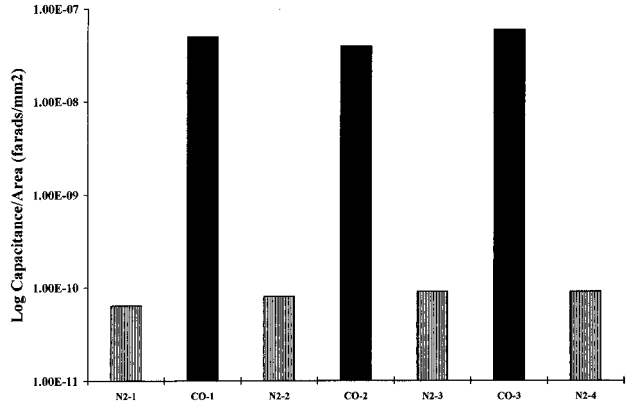

Figure 14. Plot of capacitance/area (farads/mm^2) for three room-temperature N_2/CO adsorption cycles by $AlPO_4$-5 (320 nm thick and 10^{-12} A/mm^2).

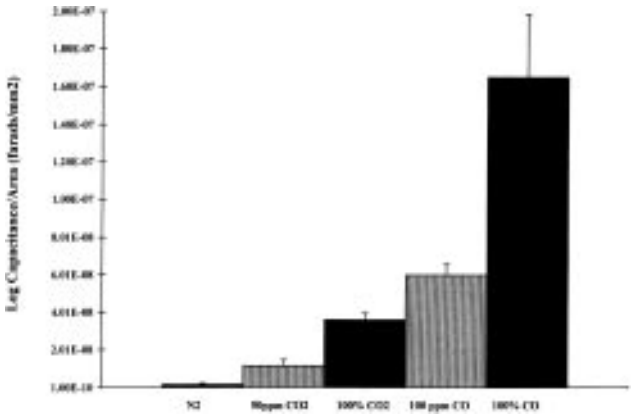

Figure 15. Plot of capacitance/area (farads/mm^2) for $AlPO_4$-5 upon room-temperature exposure to N_2, 50 ppm CO_2, 100% CO, 100 ppm CO, and 100% CO (320 nm thick and 10^{-12} A/mm^2 leakage current and +0.3 V).

Figure 13 shows a plot of the room-temperature capacitance changes of five N_2/CO_2 adsorption cycles with an $AlPO_4$-5 based capacitor having a thickness of 320 nm at a potential of 0.3 V. With each nitrogen purge the capacitance returned to $(6.4 \pm 0.12) \times 10^{-11}$ farads/mm^2 and with each exposure to pure CO_2 the capacitance increased to $(4.6 \pm 3.5) \times 10^{-8}$ farads/mm^2.

The $AlPO_4$-5 sensor (320 nm thick) response to pure CO under the same conditions was also reversible as shown in Figure 14. The capacitor was exposed to CO three times, and after each exposure there was a subsequent purge of nitrogen for 10 min. These results differ from CoAPO-5 which had a longer recovery time.[15] For the CoAPO-5 based sensor after 20 min the sensor was only 30% reversible; however, after subsequent heating to 200 °C the capacitance of the sensor returned to the original N_2 capacitance. A commercially viable CO or CO_2 sensor for combustion gas monitoring needs to have a minimum lifetime of 3 years, which generally translates into ~30 reversible cycles. $AlPO_4$-5 was shown to be reversible for H_2O, CO_2, and CO for at least five cycles, while longer term stability studies are in progress.

Reproducibility in terms of our fabrication of thin films that exhibit the same response to a target molecule is an important issue. Therefore, we prepared 10

samples with a thickness of 208 ± 21 nm. Each sample was exposed to N_2, 50 ppm CO_2, pure CO_2, 100 ppm CO, and pure CO, and the capacitance measured with a N_2 purge before exposure to each gas. Figure 15 shows a plot of the capacitance changes for sensors with an average $AlPO_4$-5 thickness of 208 nm thick at a potential of +0.3 V. The deviations of capacitance as a function of different sensors with different thickness fall within experimental error. For example the calculated capacitance ($C = \epsilon A/d$) for a capacitor with $d = 200$ and $d = 230$ falls below the experimental error. A commercially viable CO_2 sensor should be able to detect as low as 800−1400 ppm concentrations. Figure 15 illustrates that the $AlPO_4$-5 sensor can detect 50 ppm levels of CO_2 with a capacitance of 10^2 farads greater than N_2. Furthermore, a commercially viable CO sensor should be able to detect as low as 80−300 ppm concentrations. Figure 15 also demonstrates that $AlPO_4$-5 based sensor can detect 100 ppm levels of CO with a capacitance of 10^2 above N_2. Furthermore, it is important that our sensor can detect low concentrations of CO when high concentrations of CO_2, H_2O, and N_2 are present. Although we have not tested our device in a mixture of these gases such as a CO/CO_2 mixture, it is evident from Figure 15 that our device should meet this requirement since it exhibits a larger change for 100 ppm CO than for pure CO_2.

Conclusions

Partially crystalline $AlPO_4$-5 molecular sieves have been shown to be sensitive materials for capacitance type gas sensors used to detect N_2, CO, and CO_2. The average CO_2 to N_2 and CO to N_2 capacitance ratios for sensors with an average thickness of 208 nm were found to be 20 and 85, respectively. The CO/CO_2 capacitance ratio for $AlPO_4$-5 is the smallest ratio for all the AFI topology[1] molecular sieves studied so far (CoAPO-5, MnAPO-5, and VAPO-5) such that the dipolar interactions with the metal aluminum phosphate surface are clearly not as great as when partial charge is introduced into the lattice. Further study of the effect of framework structure and composition on the dielectric properties are in progress. Future work will include the study of additional MeAPOs such as CrAPO, FeAPO, and ZnAPO. These results have furthered our objective to produce a capacitance type device with an array of these molecular sieves in order to identify gases in a complex mixture.

Acknowledgment. We wish to thank the National Science Foundation and Texas Instruments, Inc. for financial support of this work.

CM960041N